

Communication

# Molecular Dynamics-Based Cohesive Zone Model for Mg/Mg<sub>17</sub>Al<sub>12</sub> Interface

Xiao Ru Zhuo <sup>1,2</sup> and Aibin Ma <sup>1,2,\*</sup>

<sup>1</sup> College of Mechanics and Materials, Hohai University, Nanjing 210098, China; xrzhuo@hhu.edu.cn

<sup>2</sup> Suqian Research Institute, Hohai University, Suqian 223800, China

\* Correspondence: aibin-ma@hhu.edu.cn; Tel.: +86-025-8378-7239

Received: 4 June 2020; Accepted: 22 June 2020; Published: 24 June 2020



**Abstract:** The fracture of the Mg/Mg<sub>17</sub>Al<sub>12</sub> interface was investigated by molecular dynamics simulations. The interface crack extends in a brittle manner without noticeable plasticity. The distributions of normal stress and separation along the interface were examined to render a quantitative picture of the fracture process. A normal traction–separation curve was extracted from simulation and compared with three cohesive zone models, i.e., cubic polynomial cohesive zone model, exponential cohesive zone model, and bilinear cohesive zone model. The exponential cohesive zone model exhibits the best agreement with simulation results, followed by the bilinear cohesive zone model.

**Keywords:** molecular dynamics simulation; cohesive zone model; Mg/Mg<sub>17</sub>Al<sub>12</sub> interface; fracture

## 1. Introduction

As one of the lightest structural materials, magnesium (Mg) alloys have attracted substantial interest from both the scientific community and various industries such as transportation and aerospace, due to their high specific strength, excellent castability, and superior damping capacity [1–3]. However, compared to structural materials such as steel, titanium and aluminum alloys, their fracture toughness is lower, which restricts their applications. It has been reported that the matrix/precipitate interface in Mg alloys is the potential site for crack nucleation [4,5]. Therefore, it is of enormous significance to investigate the fracture properties of the matrix/precipitate interface.

Cohesive zone models (CZMs), which were first proposed by Dugdale [6] and Barenblatt [7], have been widely employed to study interfacial fracture. In the framework of CZM, fracture is described by a traction–separation relation, which is typically obtained based on macroscale fracture properties such as fracture strength and toughness. Such traction–separation relations represent the collective response of all microstructure constituents within the specimen, rather than the unique response of the interface where fracture takes place [8]. To establish a CZM that can capture the local response in the vicinity of a crack, one needs to have the knowledge of local nanoscale properties, which can be obtained through molecular dynamics (MD) simulations. After the pioneering work of Gall et al. [9] that parameterized CZMs for Al/Si bimaterial by using MD simulation results as input, substantial efforts have been devoted to developing MD-based CZMs for various materials, including Al grain boundary [8], SiC/Mg nanocomposite [10], Fe single crystal [11], Al/Si bimaterials [12], and FCC single crystals [13]. However, despite numerous efforts, no attention has been paid to the fracture of the matrix/precipitate interface in Mg alloys.

In this work, we investigated by MD simulations the fracture of the Mg/Mg<sub>17</sub>Al<sub>12</sub> interface, which is commonly found in commercial Mg–Al alloys. Tensile loading was applied to the bimaterial with an interface crack to initiate crack propagation. The evolution of atomic configuration during tensile

loading was visualized to reveal the fracture mechanism. The traction–separation relation for the Mg/Mg<sub>17</sub>Al<sub>12</sub> interface was extracted from MD simulations and then compared with three CZMs.

## 2. Materials and Methods

As shown in Figure 1, the simulation model has a dimension of 38.7 ( $w$ )  $\times$  29.6 ( $h$ )  $\times$  14.6 ( $t$ ) nm, with the Mg<sub>17</sub>Al<sub>12</sub> precipitate and Mg matrix orientated such that (0001)<sub>M</sub>//(110)<sub>P</sub>, [−2110]<sub>M</sub>//[1−11]<sub>P</sub>, [01−10]<sub>M</sub>//[−112]<sub>P</sub>, satisfying the well-known Burgers orientation relationship [14]. The precipitate, which has a BCC structure with 58 atoms per unit cell, was constructed according to the structure given by Gharghouri et al. [15]. An interface crack of length  $c$  was inserted into the simulation system by blocking the interactions between atoms above and below crack surfaces, followed by a relaxation process by the conjugate gradient method. Then, boundary atoms (shaded by light orange) were frozen, whereas active atoms (all atoms except boundary atoms) were equilibrated in the NVT ensemble at 1 K for 20 ps. Subsequently, a mode I loading with a strain rate of  $6.8 \times 10^8 \text{ s}^{-1}$  was applied to the bimaterial by moving the two boundaries oppositely along the  $z$ -axis. We have checked the possible effects arising from model size and determined that the current model is large enough to yield steady state propagation.

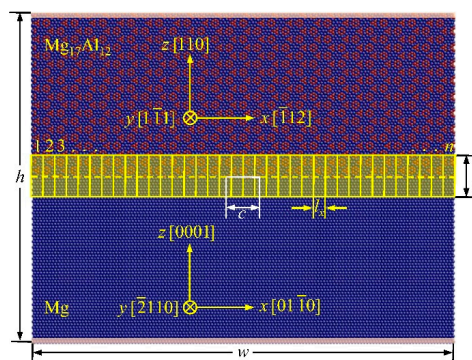


Figure 1. Simulation model of the Mg/Mg<sub>17</sub>Al<sub>12</sub> bimaterial.

MD simulations were carried out using the large-scale atomic/molecular massively parallel simulator (LAMMPS) [16] with a timestep of 1 fs. Atomeye, which is an atomistic configuration viewer developed by Li [17], was used to visualize atomic configurations. The Mg–Mg, Al–Al, Mg–Al atomic interactions were described by the embedded atom method (EAM) potential [18]. The stress tensor of the simulation system was calculated according to the definition of virial stress. A horizontal layer (shaded by light yellow in Figure 1) consisting of half Mg and half Mg<sub>17</sub>Al<sub>12</sub> was divided into  $n$  (45) small regions, each of which is a cohesive zone volume element (CZVE) [8], with a dimension of  $0.9 (l_x) \times 2.1 (l_z) \times 14.6 (t)$  nm. Two variables were used to monitor the state of each CZVE, i.e.,  $T_n$  and  $u_n$ .  $T_n$  is the average atomic stress  $\sigma_{zz}$  of all atoms in each CZVE, while  $u_n$  is the average atomic displacement  $\Delta z$  of all atoms in the Mg<sub>17</sub>Al<sub>12</sub> half with reference to the Mg half.

## 3. Results

The atomic configuration evolution of the bimaterial as the increase of strain is shown Figure 2, with atoms colored according to the  $zz$  component of the atomic stress. Due to its hexagonal close-packed (HCP) structure, the available deformation mode in Mg is limited, leading to its relatively low ductility [19]. In this study, tensile loading along the [0001] direction, which is the  $\langle c \rangle$  axis of Mg, was applied to the simulation system. At room temperature, the  $\langle c + a \rangle$  slip system is difficult to activate because of its high critical resolved shear stress, and therefore, twinning is the primary mechanism to accommodate plastic deformation in the  $\langle c \rangle$  axis [19]. However, neither twinning nor any dislocation activity was observed in our simulations. Instead, the interface crack was observed to propagate in a brittle manner without any noticeable plasticity, despite crack surfaces not being very

clean, as shown in Figure 2. This finding is consistent with the previous experimental observation that decohesion occurs in the Mg/precipitate interface [5]. Due to the existence of the inserted interface crack, stress concentration was induced near the crack tips, which may make crack propagation along the interface more favorable than twinning or dislocation activities. Stress concentration at the crack tips can be observed from Figure 2. In addition, simulations were carried out at a low temperature of 1 K, which might suppress plastic deformation to some extent.

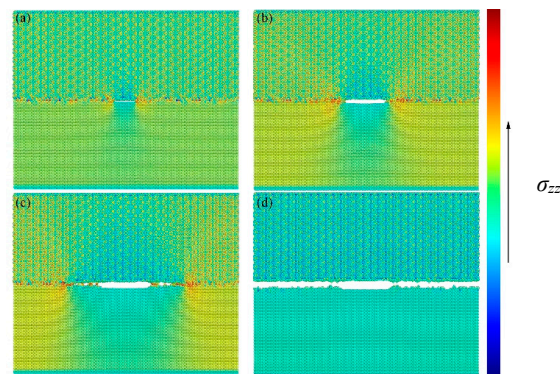


**Figure 2.** Atomistic configurations of the Mg/Mg<sub>17</sub>Al<sub>12</sub> bimaterial corresponding to different strains: (a)  $\varepsilon = 0.031$ ; (b)  $\varepsilon = 0.041$ ; (c)  $\varepsilon = 0.046$ ; (d)  $\varepsilon = 0.055$ . Atoms are colored according to the  $zz$  component of the atomic stress.

To render a general quantitative picture of the fracture process, the distribution of  $T_n$ ,  $u_n$ , and  $\Delta z$  along the interface for two strain values corresponding to Figure 2a,c is shown in Figure 3. Both  $T_n$  and  $u_n$  exhibit a near-symmetrical distribution with respect to an axis parallel to the  $z$ -axis.  $u_n$  remains constant as  $x$  varies in the bonded region and increases gradually from the crack tips to the axis of symmetry, where the maximum value is achieved. The displacement of Mg is larger than that of Mg<sub>17</sub>Al<sub>12</sub>, which is reasonable since Mg<sub>17</sub>Al<sub>12</sub> is stiffer than Mg [15].  $T_n$  reaches its maximum value at the crack tips and decreases rapidly to a nearly constant value for the bonded interface away from the crack tips.  $T_n$  is zero for the cracked interface. The overall distribution of  $T_n$  and  $u_n$  is generally consistent with the prediction of linear elastic fracture mechanics [20]. A similar observation was reported in previous studies on the fracture of Al/Si interfaces [12] and interfaces composed of BCC materials [21]. It can be noted from Figure 3 that the interface crack has propagated for a certain distance when  $\varepsilon$  increases from 0.031 to 0.046, in agreement with the observation in Figure 2.

The  $T_n - u_n$  curve was extracted from simulation, as shown in Figure 4.  $T_n$  increases nearly linearly as  $u_n$  increases, until reaching the maximum value which is known as cohesive strength  $\sigma_c$  (corresponding  $u_n$  is denoted by  $\delta_c$ ), followed by a descending trend to zero. The  $u_n$  at which  $T_n$  reduces to zero is  $\delta_s$ , indicating the complete separation of the interface. The  $T_n - u_n$  curve extracted from MD simulation was compared with that predicted by three widely used CZMs, namely cubic polynomial CZM [22], exponential CZM [23], and bilinear CZM [24]. In the cubic polynomial CZM,  $T_n$  is related to  $u_n$  by

$$T_n = \begin{cases} \frac{27}{4} \sigma_c \frac{u_n}{\delta_s} \left(1 - \frac{u_n}{\delta_s}\right)^2 & \text{for } u_n \leq \delta_s \\ 0 & \text{for } u_n > \delta_s \end{cases} \quad (1)$$

$T_n$  for the exponential CZM is expressed as

$$T_n = \frac{16}{9} \sigma_c e^2 \frac{u_n}{\delta_s} \exp\left(-\frac{16}{9} e \frac{u_n}{\delta_s}\right) \quad (2)$$

In the bilinear CZM, is given as

$$T_n = \begin{cases} \sigma_c \frac{\delta_s - u_n^*}{\delta_s - \delta_c} \frac{u_n}{u_n^*} & \text{for } u_n \leq \delta_s \\ 0 & \text{for } u_n > \delta_s \end{cases} \quad (3)$$

where  $u_n^* = \max(\delta_c, u_n)$ . Note from Equations (1)–(3) that cubic polynomial and exponential CZMs are associated with two parameters ( $\sigma_c$  and  $\delta_s$ ), while bilinear CZM is related to one more parameter  $\delta_c$ . These three parameters were obtained from MD simulation as  $\sigma_c = 5.63$  GPa,  $\delta_s = 7.80$  Å,  $\delta_c = 1.53$  Å, which were then input to Equations (1)–(3) to plot  $T_n$ – $u_n$  curves, as shown in Figure 4. Exponential CZM exhibits the best agreement with MD results since it can capture the nonlinear processes associated with bond breaking.

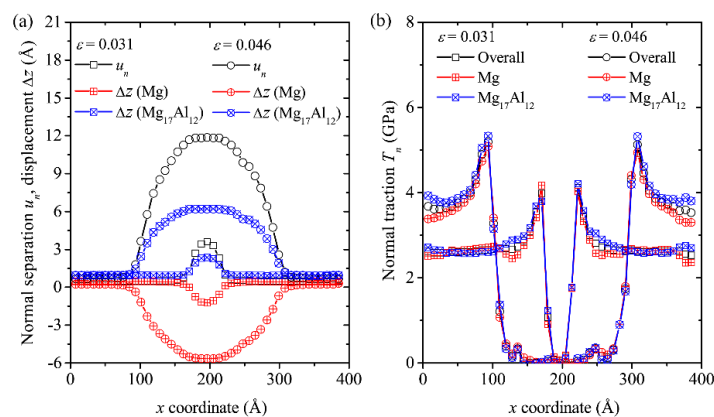


**Figure 3.** (a) Distribution of normal separation  $u_n$  and displacement  $\Delta z$  along the interface for two different strains. “ $\Delta z$  (Mg)” and “ $\Delta z$  ( $Mg_{17}Al_{12}$ )” are the average atomic displacement  $\Delta z$  of all atoms in the “Mg” half and “ $Mg_{17}Al_{12}$ ” half of an CZVE, respectively. (b) Distribution of normal traction  $T_n$  along the interface for two different strains. “Overall” indicates the average atomic stress  $\sigma_{zz}$  of all atoms in each CZVE. “Mg” and “ $Mg_{17}Al_{12}$ ” are the average atomic stress  $\sigma_{zz}$  of all atoms in the “Mg” half and “ $Mg_{17}Al_{12}$ ” half of an CZVE, respectively.

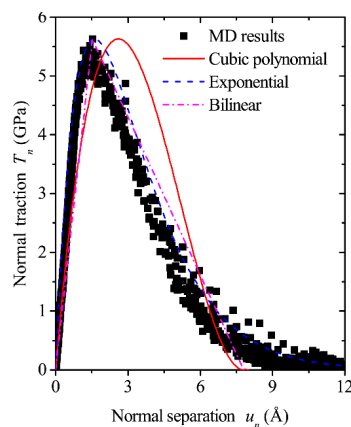


**Figure 4.** Normal traction–separation curves obtained from MD simulations and predicted by cohesive zone models.

#### 4. Conclusions

MD simulations were performed to investigate the fracture of Mg/ $Mg_{17}Al_{12}$  interface. The interface crack extended in a brittle manner without noticeable plasticity. The expressions for three CZMs were established by using parameters obtained from MD simulations. The normal traction–separation curves predicted by the three CZMs were compared with that extracted from MD simulations. Exponential CZM shows the closest match with MD results, followed by bilinear CZM.

**Author Contributions:** Visualization, Investigation, Writing—original draft: X.R.Z.; Writing—review & editing, Supervision: A.M. All authors have read and agreed to the published version of the manuscript.

**Funding:** This research was supported by the Fundamental Research Funds for the Central Universities (B200202132), the China Postdoctoral Science Foundation (Grant No. 2018M632214), and the Guiding Capital for Industry Development Project of Suqian of China (Grant No. H201817).

**Conflicts of Interest:** The authors declare no conflict of interest.

## References

1. Ou, K.-L.; Chen, C.-C.; Chiu, C. Production of oxide dispersion strengthened Mg-Zn-Y alloy by equal channel angular pressing of mechanically alloyed powder. *Metals* **2020**, *10*, 679. [[CrossRef](#)]
2. Wang, C.; Ma, A.; Sun, J.; Zhuo, X.; Huang, H.; Liu, H.; Yang, Z.; Jiang, J. Improving strength and ductility of a Mg-3.7Al-1.8Ca-0.4Mn alloy with refined and dispersed Al<sub>2</sub>Ca particles by industrial-scale ECAP processing. *Metals* **2019**, *9*, 767. [[CrossRef](#)]
3. Sun, J.; Yang, Z.; Liu, H.; Han, J.; Wu, Y.; Zhuo, X.; Song, D.; Jiang, J.; Ma, A.; Wu, G. Tension-compression asymmetry of the AZ91 magnesium alloy with multi-heterogenous microstructure. *Mater. Sci. Eng. A* **2019**, *759*, 703–707. [[CrossRef](#)]
4. Cui, X.; Yu, Z.; Liu, F.; Du, Z.; Bai, P. Influence of secondary phases on crack initiation and propagation during fracture process of as-cast Mg-Al-Zn-Nd alloy. *Mater. Sci. Eng. A* **2019**, *759*, 708–714. [[CrossRef](#)]
5. Baek, S.M.; Park, H.K.; Yoon, J.I.; Jung, J.; Moon, J.H.; Lee, S.G.; Kim, J.H.; Kim, T.S.; Lee, S.; Kim, N.J.; et al. Effect of secondary phase particles on the tensile behavior of Mg-Zn-Ca alloy. *Mater. Sci. Eng. A* **2018**, *735*, 288–294. [[CrossRef](#)]
6. Dugdale, D.S. Yielding of steel sheets containing slits. *J. Mech. Phys. Solids* **1960**, *8*, 100–104. [[CrossRef](#)]
7. Barenblatt, G.I. The mathematical theory of equilibrium cracks in brittle fracture. *Adv. Appl. Mech.* **1962**, *7*, 55–129. [[CrossRef](#)]
8. Yamakov, V.; Saether, E.; Phillips, D.R.; Glaessgen, E.H. Molecular-dynamics simulation-based cohesive zone representation of intergranular fracture processes in aluminum. *J. Mech. Phys. Solids* **2006**, *54*, 1899–1928. [[CrossRef](#)]
9. Gall, K.; Horstemeyer, M.F.; Van Schilfgaarde, M.; Baskes, M.I. Atomistic simulations on the tensile debonding of an aluminum-silicon interface. *J. Mech. Phys. Solids* **2000**, *48*, 2183–2212. [[CrossRef](#)]
10. Zhou, X.; Bu, W.; Song, S.; Sansoz, F.; Huang, X. Multiscale modeling of interfacial mechanical behaviours of SiC/Mg nanocomposites. *Mater. Des.* **2019**, *182*, 108093. [[CrossRef](#)]
11. Xu, T.; Stewart, R.; Fan, J.; Zeng, X.; Yao, A. Bridging crack propagation at the atomistic and mesoscopic scale for BCC-Fe with hybrid multiscale methods. *Eng. Fract. Mech.* **2016**, *155*, 166–182. [[CrossRef](#)]
12. Zhuo, X.R.; Ma, A.; Beom, H.G. Cohesive zone representation of interfacial fracture in aluminum-silicon biomaterials. *Comput. Mater. Sci.* **2019**, *169*, 109105. [[CrossRef](#)]
13. Lee, G.H.; Kim, J.H.; Beom, H.G. Cohesive zone modeling of crack propagation in FCC single crystals via atomistic simulations. *Met. Mater. Int.* **2020**. [[CrossRef](#)]
14. Crawley, A.F.; Milliken, K.S. Precipitate morphology and orientation relationships in an aged Mg-9% Al-1% Zn-0.3% Mn alloy. *Acta Metall.* **1974**, *22*, 557–562. [[CrossRef](#)]
15. Gharghoury, M.A.; Weatherly, G.C.; Embury, J.D. The interaction of twins and precipitates in a Mg-7.7 at.% Al alloy. *Philos. Mag.* **1998**, *78*, 1137–1149. [[CrossRef](#)]
16. Plimpton, S. Fast parallel algorithms for short-range molecular dynamics. *J. Comput. Phys.* **1995**, *117*, 1–19. [[CrossRef](#)]
17. Li, J. AtomEye: An efficient atomistic configuration viewer. *Model. Simul. Mater. Sci. Eng.* **2003**, *11*, 173–177. [[CrossRef](#)]
18. Liu, X.Y.; Ohotnicky, P.P.; Adams, J.B.; Rohrer, C.L.; Hyland, R.W. Anisotropic surface segregation in Al-Mg alloys. *Surf. Sci.* **1997**, *373*, 357–370. [[CrossRef](#)]
19. Barnett, M.R. Twinning and the ductility of magnesium alloys. *Mater. Sci. Eng. A* **2007**, *464*, 1–7. [[CrossRef](#)]
20. Farahmand, B.; Bockrath, G.; Glassco, J. Linear Elastic Fracture Mechanics. In *Fatigue and Fracture Mechanics of High Risk Parts*; Springer: Boston, MA, USA, 1997. [[CrossRef](#)]

21. Zhou, X.W.; Moody, N.; Jones, R.; Zimmerman, J.; Reedy, E. Molecular-dynamics-based cohesive zone law for brittle interfacial fracture under mixed loading conditions: Effects of elastic constant mismatch. *Acta Mater.* **2009**, *57*, 4671–4686. [[CrossRef](#)]
22. Needleman, A. A continuum model for void nucleation by inclusion debonding. *J. Appl. Mech.* **1987**, *54*, 525–531. [[CrossRef](#)]
23. Needleman, A. An analysis of tensile decohesion along an interface. *J. Mech. Phys. Solids* **1990**, *38*, 289–324. [[CrossRef](#)]
24. Geubelle, P.H.; Baylor, J.S. Impact-induced delamination of composites: A 2D simulation. *Compos. B Eng.* **1998**, *29*, 589–602. [[CrossRef](#)]



© 2020 by the authors. Licensee MDPI, Basel, Switzerland. This article is an open access article distributed under the terms and conditions of the Creative Commons Attribution (CC BY) license (<http://creativecommons.org/licenses/by/4.0/>).